EXPERIMENTAL TESTING AND INVESTIGATION OF THE STRESS-DEPENDENT MATERIAL BEHAVIOUR OF ASPHALT VIA THE TRIAXIAL TEST

A. ZEIßLER & F. WELLNER
Institute of Urban and Road Engineering (IURE), Technische Universität Dresden, Germany
alexander.zeissler@tu-dresden.de
I. WOLLNY & C. ZOPF & M. KALISKE
Institute for Structural Analysis (ISD), Technische Universität Dresden, Germany
ines.wollny@tu-dresden.de

ABSTRACT

Highly developed numerical simulations demand not only for efficient algorithms and constitutive material formulations, but also for reliable experimental data in order to represent the mechanical material behavior in an adequate way. The Repeated Load Triaxial (RLT) test is a suitable testing methodology to investigate the mechanical properties of asphalt mixes under cyclic loading.

This triaxial test is based on the three-dimensional stress state especially adapted to appropriate material parameters for any pavement model, which is able to simulate the three-dimensional asphalt behaviour. The three-dimensional stress state in the triaxial test with cyclic axial and horizontal loads causes a complex strain response, so that it is impossible to determine the material parameters from one single test due to the nonlinear behaviour of asphalt. Therefore, a new approach for the interpretation of the triaxial test results is required. The basic idea of the new approach depends on the following assumption: If the functional relationship between axial and horizontal strains related to axial and horizontal stresses is known, one can determine via the derivative of this function with respect to σ_1 or σ_{23} the resilient modulus and Poisson's ratio. In context with the phase lag, it becomes possible to describe the Cole-Cole-Plot of the complex modulus in dependency on the stress state.

In result of the complex interpretation of the triaxial tests, it is possible to determine the elastic and viscoelastic material parameters for asphalt mixes. The determined material parameters can be used for the numerical simulation of pavement structures.

1. INTRODUCTION

Although careful planning and design of infrastructure projects as well as quality checks during the construction, every year a considerable number of damages occurs to the road network of the Federal Republic of Germany. These damages lead to a high risk for traffic, significant cost for maintenance and repair as well as to an environmental impact due to congestion and traffic diversion.

In order to assess the sensitivity to damage of asphalt pavements, fundamental knowledge about the material behaviour of asphalt and the interaction of tires and pavements is required. By means of numerical models, the efficient prediction of damage and life cycle of pavements becomes possible. These models allow a realistic mapping of the structural behaviour of the tire and the pavement as well as the consideration of the temperature and stress dependent behaviour of tire and pavement materials.

In Order to investigate the interaction phenomena of coupled tire and pavement structures under consideration of flexible pavement structures, a research project supported by the German Research Foundation (DFG) was and is carried out. This research project is be conducted in cooperation of IURE and ISD of Technische Universität Dresden. The main goal of the first project phase is the generation of general mechanical understanding of the complex interactions of the tire-pavement-system including the investigation of the complex material behavior of asphalt. In this context, the presented results of this paper refer to the phenomenologically based laboratory test results and the stress dependent anisotropic material behavior of stone mastic asphalt (SMA 11 S with PmB 25/55-55A).

2. PHENOMENOLOGICALLY BASED LABORATORY TESTS

2.1. Material Testing Methodologies

Prerequisite for any successful analytical / numerical design methodology is the acquisition of reliable measurements from representative experimental investigations (e.g. see Fig. 1 and Fig. 2) followed by appropriate mathematical characterization of the deformation behaviour of bound and unbound layers in the pavement structure. As far as the fatigue behaviour of asphalt mixes is concerned, a wide range of experimental data and fatigue models is available [1], [2], [3]. The situation regarding the behaviour of asphalt mixes with respect to the elastic and viscoelastic properties as well as the accumulation of plastic deformation under repeated traffic loads is much less well developed. In addition, less experience is available to compare the fatigue curves for asphalt mixes using different fatigue testing methodologies.

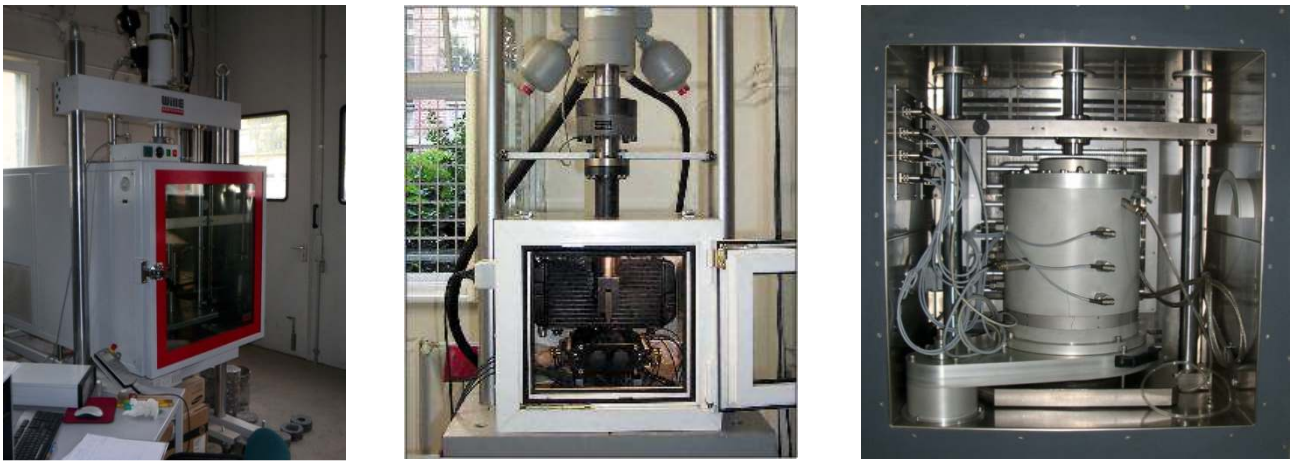

Fig. 1: Direct Tensile Test, Indirect Tensile Test and Triaxial Test machine (at IURE)

The Repeated Load Triaxial (RLT) test is a suitable testing methodology to investigate the mechanical properties of asphalt mixes under dynamic loading. A research project at IURE was aimed at investigating long term performance of asphalt mixes using different testing methodologies, e.g. RLT test, Direct Tensile Test (DTT), Indirect Tensile Test (ITT). The RLT test is a new and innovative testing method for asphalt mixes. First positive experience was gained during this research project [4].

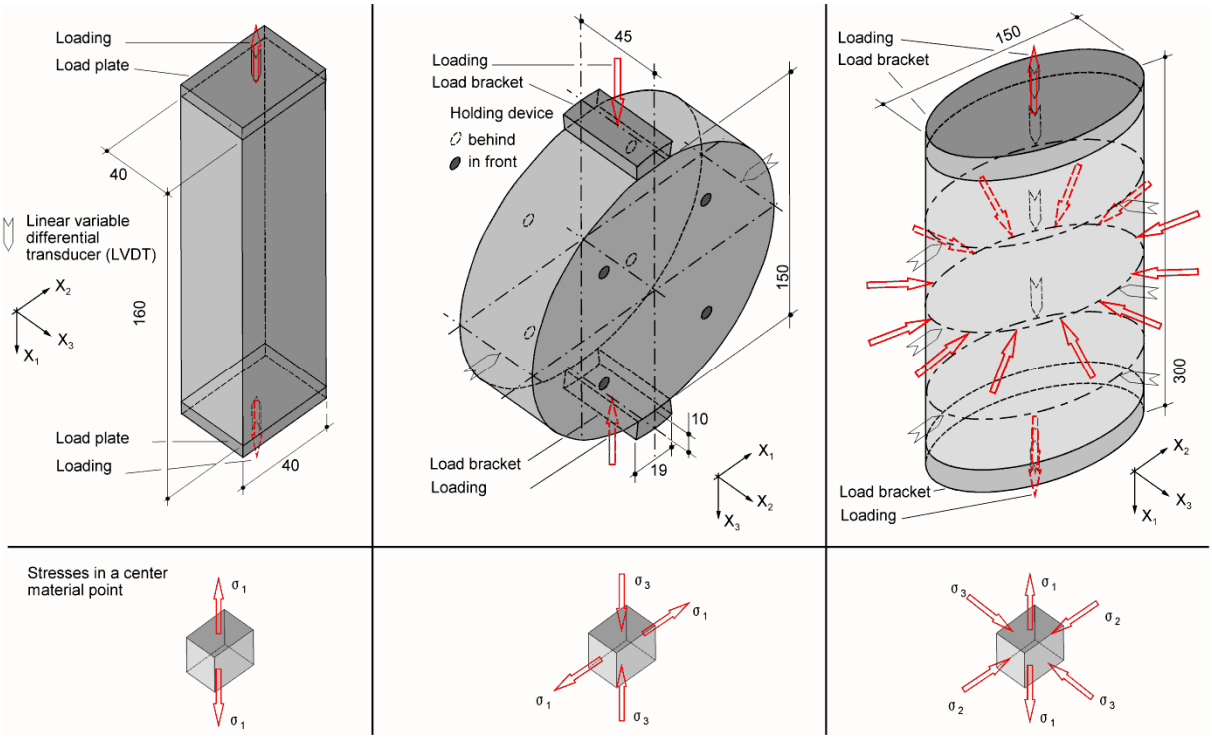

Fig. 2: Test samples and stresses in a centre material point

2.2. Triaxial Testing Methodology

The triaxial test is based on the three-dimensional stress state especially adapted to appropriate material parameters for the asphalt pavement model, which is able to simulate the three-dimensional interaction between tires and pavement.

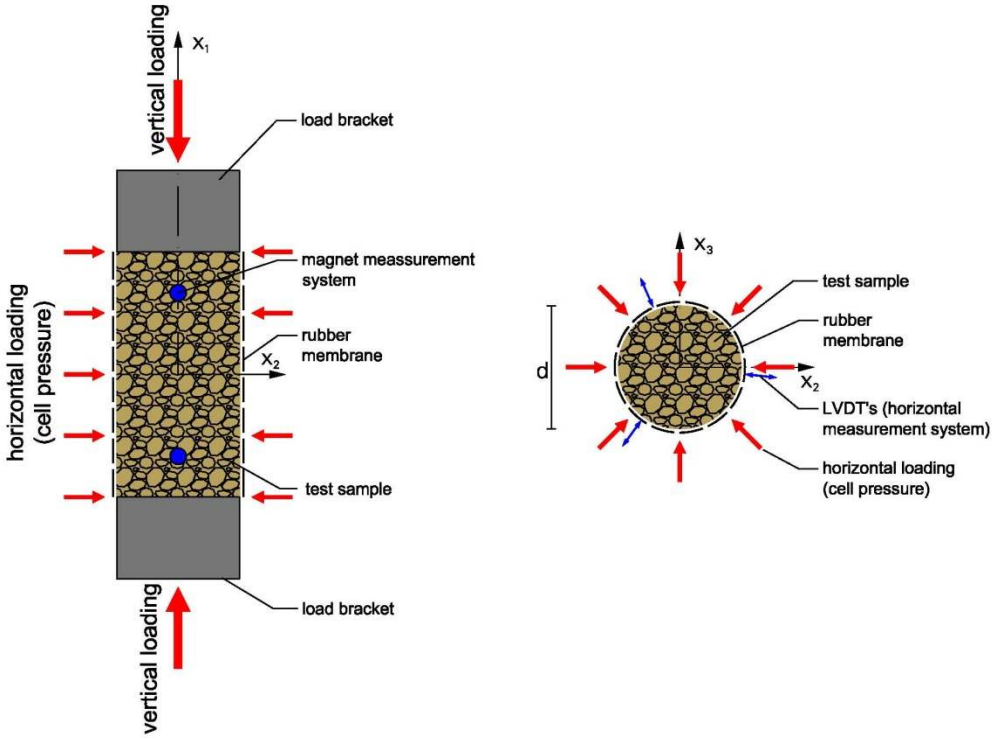

Fig. 3: Schematical configuration of the triaxial apparatus used at TU Dresden (Institute of Urban and Road Engineering – IURE) for the triaxial tests

Fig. 3 shows the schematical configuration of the triaxial apparatus, which is used for the investigations at TU Dresden.

The three-dimensional stress state in the triaxial test with cyclic axial and horizontal loads causes a complex strain reaction, so that it is impossible to determine the material parameters from one single test due to the nonlinear behaviour of asphalt. Therefore, a new approach in the interpretation of the triaxial test results is necessary. The basic idea of the new approach depends on the following assumption: If the functional relationship between axial and horizontal strains related to axial and horizontal stresses is known, one can determine via the derivative of this function with respect to σ_1 or σ_{23} the resilient modulus and Poisson's ratio. The approach will be described in detail below.

2.3. Anisotropic Material Behaviour of Asphalt

For the preparation of the asphalt test samples in the laboratory, a Roller Sector Compactor is used. In the first step, an asphalt sample was prepared. The compaction load is applied vertically. During the compaction process, the mineral particles mainly orientate horizontally (see Fig. 4). Thus, the behaviour of asphalt can be assumed to be anisotropic.

In the second step, cylindrical test samples are taken by drilling them from the asphalt sample. These cylindrical test samples are sawn to the appropriate height and are used for the experiments.

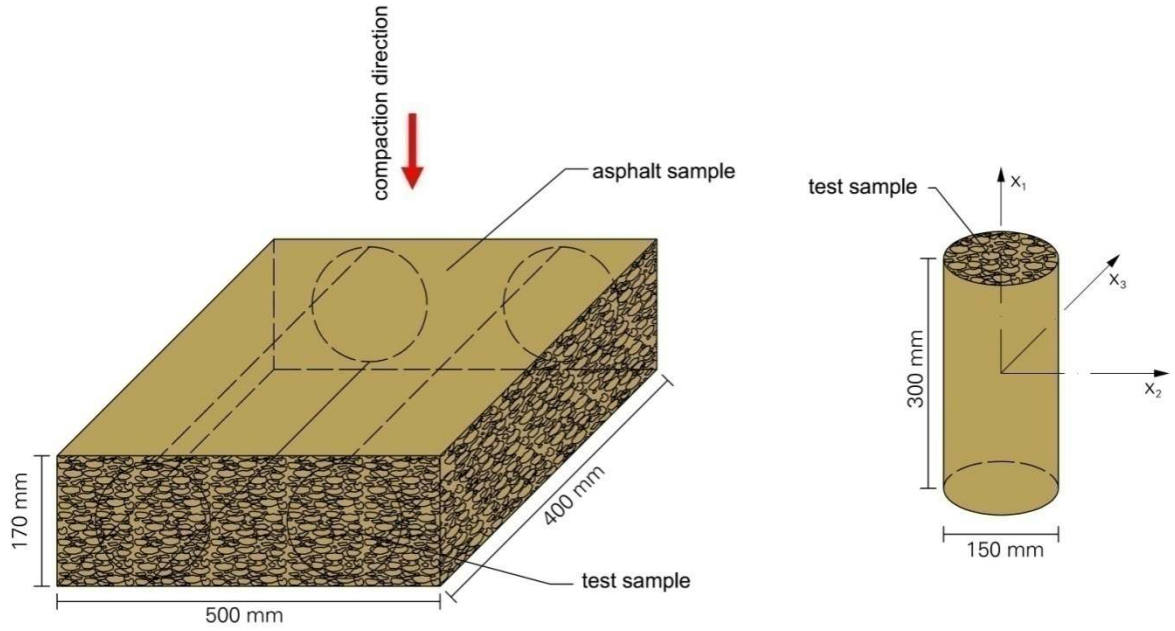

Fig. 4: Preparation of hot rolled asphalt test samples

Based on the assumption that the behaviour is anisotropic, the three equations

$$\varepsilon_1 = \frac{\sigma_1}{|E_1|} - \mu_{12}\frac{\sigma_2}{|E_2|} - \mu_{13}\frac{\sigma_3}{|E_3|}, \tag{1}$$

$$\varepsilon_2 = \frac{\sigma_2}{|E_2|} - \mu_{21}\frac{\sigma_1}{|E_1|} - \mu_{23}\frac{\sigma_3}{|E_3|}, \tag{2}$$

$$\varepsilon_3 = \frac{\sigma_3}{|E_3|} - \mu_{31}\frac{\sigma_1}{|E_1|} - \mu_{32}\frac{\sigma_2}{|E_2|} \tag{3}$$

are accordingly applied.

For the interpretation of the tests, one simplification is made. The anisotropy relates to the x_1-x_2 respectively x_1-x_3-plane. In result, the axis-symmetric stress state is determined using

$$|E_2| = |E_3| = |E_{23}|,\ \varepsilon_2 = \varepsilon_3 = \varepsilon_{23},\ \mu_{12} = \mu_{21} = \mu_{13} = \mu_{31} = \mu_1,\ \mu_{23} = \mu_{32},\ \sigma_2 = \sigma_3 = \sigma_{23},$$

$$\varepsilon_1 = \frac{\sigma_1}{|E_1|} - 2\mu_1\frac{\sigma_{23}}{|E_{23}|}, \tag{4}$$

$$\varepsilon_{23} = \frac{\sigma_{23}}{|E_{23}|}(1-\mu_{23}) - \mu_1\frac{\sigma_1}{|E_1|}. \tag{5}$$

3. INTERPRETATION OF TRIAXIAL TEST RESULTS

3.1. Nonlinear Material Behaviour of Asphalt

The trend of the strain-function in dependency of σ_1 and σ_{23} is exemplary shown in Fig. 5 and Fig. 6 for a test temperature of 25 °C and for a test frequency of 1 Hz. If the amplitude of one of the stress components is constant, then the trend is linear. The variation of both stress components σ_1 and σ_{23} tends to result in a change of the increase of the strain-function, hence a nonlinear and stress-dependent behaviour can be assumed.

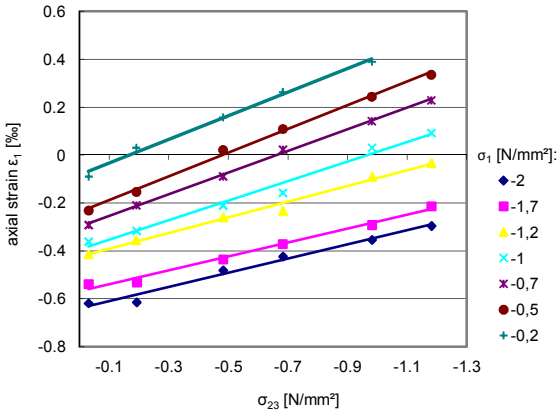

Fig. 5: Relationship between σ_{23} and ε_1 for f = 1 Hz and T = 25 °C for a constant amplitude of σ_1

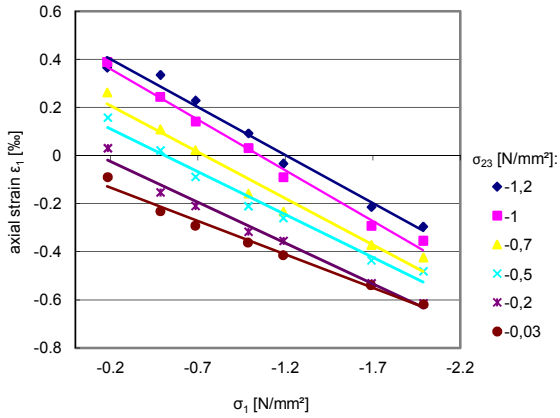

Fig. 6: Relationship between σ_1 and ε_1 for f = 1 Hz and T = 25 °C for a constant amplitude of σ_{23}

Equations (4) and (5) contain three and four unknown variables, respectively. Thus, the calculation of the dynamic modulus as well as Poisson's ratio cannot be done directly. The generation of a system of equations from differing tests with variation of σ_1 and σ_{23} is also not possible due to the nonlinearity.

3.2. Interpretation of the Triaxial Test via Derivative of the Surface Function

Adapted from the linear trend of the strain-function with one constant component of strain and the basic condition, that for $\sigma_1 = 0$ and $\sigma_{23} = 0$ also ε_1 respectively ε_{23} equal 0, the functional approach for the surface function of axial strain

$$\varepsilon_1 = f(\sigma_1, \sigma_{23}) = a_1 \cdot \sigma_1 + a_2 \cdot \sigma_{23} + a_3 \cdot \sigma_1 \cdot \sigma_{23} \tag{6}$$

and the radial strain

$$\varepsilon_{23} = f(\sigma_1, \sigma_{23}) = a_{1,23} \cdot \sigma_1 + a_{2,23} \cdot \sigma_{23} + a_{3,23} \cdot \sigma_1 \cdot \sigma_{23} \tag{7}$$

in dependency of the axial stress σ_1 and the cell pressure σ_{23} is postulated. The variables a_1, a_2, a_3, $a_{1,23}$, $a_{2,23}$, $a_{3,23}$ are parameters of the surface function and temperature- and frequency-dependent.

In Fig. 7, the surface plot of ε_1 at f = 1 Hz und T = 25 °C is shown.

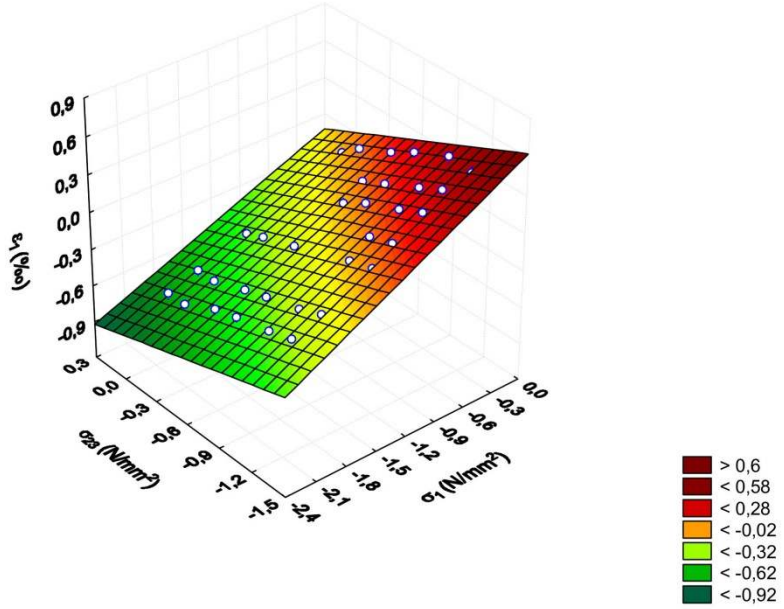

Fig. 7: Surface plot of ε_1 versus σ_1 and σ_{23} at f = 1 Hz and T = 25 °C

From the derivative of Equation (4) with respect to σ_1

$$\frac{d\varepsilon_1}{d\sigma_1} = \frac{1}{|E_1|} \tag{8}$$

related to the derivative of the surface function (6) with respect to σ_1

$$\frac{d\varepsilon_1}{d\sigma_1} = a_1 + a_3 \cdot \sigma_{23} = \frac{1}{|E_1|}, \tag{9}$$

the reciprocal value of the dynamic modulus in axial direction can be calculated. After rearranging Equation (9), the absolute value of the complex modulus $|E_1|$

$$|E_1| = \frac{1}{a_1 + a_3 \cdot \sigma_{23}} \tag{10}$$

can be calculated with the parameters a_1, a_3 and the stress component σ_{23}. The derivative of Equation (5) with respect to σ_1 delivers

$$\frac{d\varepsilon_{23}}{d\sigma_1} = -\frac{\mu_1}{|E_1|}. \tag{11}$$

The equalization of Equation (10) with derivative of Equation (5) with respect to σ_1 delivers

$$\mu_1 = -(a_{1,23} + a_{3,23} \cdot \sigma_{23}) \cdot |E_1|. \tag{12}$$

From the derivative of Equation (4) with respect to σ_{23} follows

$$\frac{d\varepsilon_1}{d\sigma_{23}} = -\frac{2 \cdot \mu_1}{|E_{23}|}. \tag{13}$$

Resulting from (13) and the derivative of the surface function (6) with respect to σ_{23}, the absolute value of complex modulus in horizontal direction

$$|E_{23}| = -\frac{2 \cdot \mu_1}{a_2 + a_3 \cdot \sigma_1} \tag{14}$$

can be calculated.

Poisson's ratio μ_{23} can be calculated analogously with the derivative of Equations (5) and (7) with respect to σ_{23}

$$\mu_{23} = 1 - |E_{23}| \cdot (a_{2,23} + a_{3,23} \cdot \sigma_1). \tag{15}$$

With the above listed equations, the interpretation of triaxial tests becomes possible. For an accurate approximation of the surface function, it is essential to get enough supporting points, thus an extensive test scale is necessary.

3.3. Calculation of the Absolute Modulus $|E_1|$

Using the equations as described before and the interpretation of the surface function of ε_1, the absolute modulus $|E_1|$ in axial direction can be calculated.

Fig. 8 and Fig. 9 show the trends of the stiffness at T = 25 °C and T = -10 °C for three different frequencies in dependency of stress component σ_{23}.

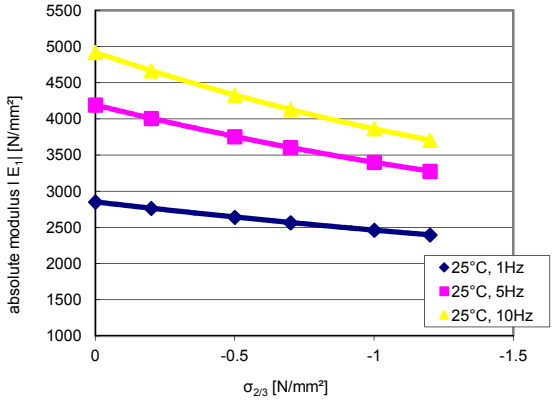

Fig. 8: Absolute modulus $|E_1|$ as a function of frequency and stress part σ_{23} at T = 25 °C

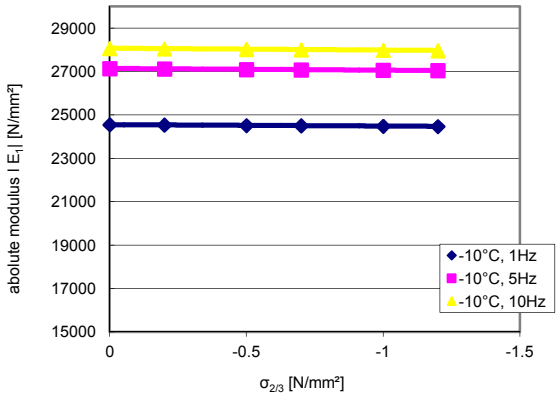

Fig. 9: Absolute modulus $|E_1|$ as a function of frequency and stress part σ_{23} at T = -10 °C

The significant different trend of the absolute modulus $|E_1|$ relating to the applied pressure σ_{23} is clearly visible. At lower temperatures, the behaviour of the asphalt test sample is close to an elastic solid as expected. A stress-dependency of the absolute modulus $|E_1|$ is unverifiable.

At T = 25 °C, an explicit stress-dependency may be detected. The stress part σ_{23} tends to result in a nonlinear stiffness trend. Phenomenologically, this behaviour is caused by the fact, that due to the viscosity of the binder the stiffness behaviour depends on temperature. Due to the cyclic loading of the support stress $\sigma_{23,}$ the bitumen film is retained in the particle-particle-contact area and reduces the direct load transfer over the granular structure. The result is the decrease of the stiffness with rising horizontal pressure. This influence depends largely upon the temperature and affects higher frequencies more than lower frequencies.

3.4. Master Curve of the Absolute Modulus $|E_1|$

Based on the interpretation of the surface function of ε_1, in Fig. 10 the master curve of the absolute modulus $|E_1|$ is shown. The derivation of used Equations (16) to (18) is described in [5]. The shift factor

$$\alpha_T = \frac{1}{e^{-m\cdot\left(\frac{1}{T+273}-\frac{1}{T_R+273}\right)}} \tag{16}$$

can be calculated with m = 25000 and T_R = 25 °C. With the aid of the corrected frequency

$$f_{korr} = f \cdot \alpha_T, \tag{17}$$

the absolute modulus

$$|E_1| = f(\log_{10}(f_{korr})) = b_1 + \frac{b_2}{1+e^{\frac{\log_{10}(f_{korr})-\left(\frac{b_3}{1+e^{b_4\cdot\sigma_{23}}}+b_5\right)}{b_6\cdot e^{b_7\cdot\sigma_{23}}+b_8}}} \tag{18}$$

can be calculated.

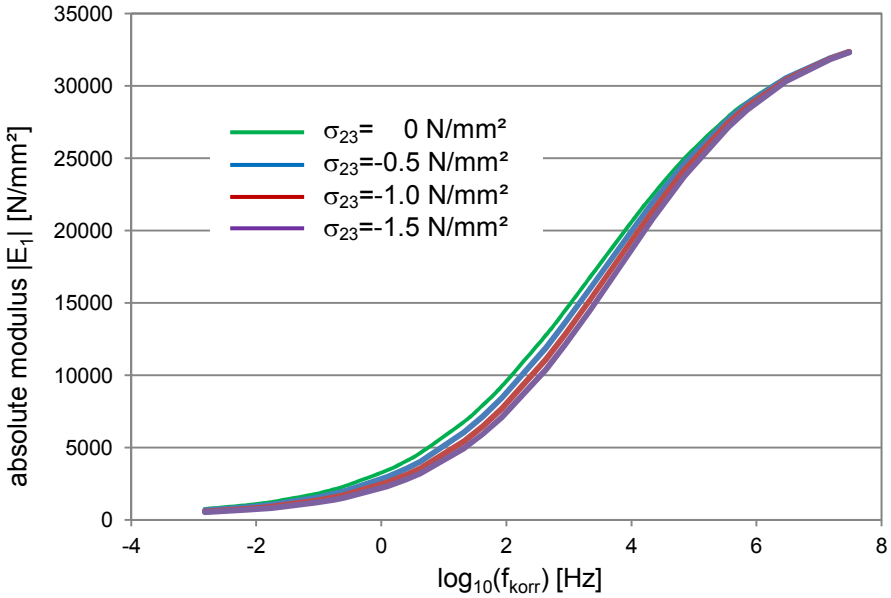

Fig. 10: Master curve of the absolute modulus $|E_1|$ with dependency on σ_{23}

The parameters of the regression function (18) are listed in Tab.1.

Tab.1: Parameters of the regression function for the absolute modulus $|E_1|$

b_1	b_2	b_3	b_4	b_5	b_6	b_7	b_8
300	34000	1,446876	0,720264	2,703742	0,188778	0,689704	1,268268

3.5. Master Curve of the Phase lags $\delta_{1(\varepsilon 1)}$ and $\delta_{2(\varepsilon 23)}$

Adequately to the already established Temperature-Frequency-Equivalence, a similar dependency is assumed to be valid for the phase lags $\delta_{1(\varepsilon 1)}$ and $\delta_{2(\varepsilon 23)}$, which describes the time lag between the axial loading and the resulting axial strain reaction respectively horizontal strain reaction.

Considering the following equations, it is possible to arrange the master curve for the phase lags, which are shown in Fig. 11.
The shift factor

$$\alpha_T = \frac{1}{e^{-m\cdot\left(\frac{1}{T+273}-\frac{1}{T_R+273}\right)}} \tag{19}$$

can be calculated analogously to (18) with m = 25000 and T_R = 25 °C. For the interpretation of the master curve of the phase lags δ using the corrected frequency

$$f_{korr} = f\cdot\alpha_T, \tag{20}$$

the following regression function

$$\delta = f(\log_{10}(f_{korr})) = b_1 + \frac{b_2}{1+e^{b_3\cdot\log_{10}(f_{korr})+b_4}} \tag{21}$$

is used.

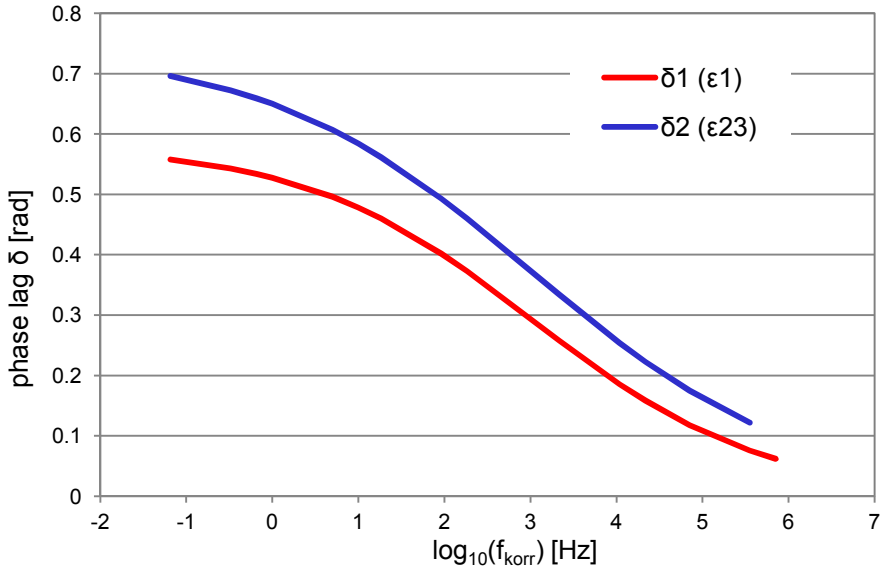

Fig. 11: Master curve of the phase lags $\delta_{1(\varepsilon 1)}$ and $\delta_{2(\varepsilon 23)}$ for $T_R = 25°C$

The parameters for the regression function (23) are listed in Tab.2 and Tab.3.

Tab.2: Parameters of the regression function of the phase lag $\delta_{1(\varepsilon 1)}$

b_1	b_2	b_3	b_4
0	0,58059	0,75653	-2,298

Tab.3: Parameters of the regression function of the phase lag $\delta_{2(\varepsilon 23)}$

b_1	b_2	b_3	b_4
0	0,74274	0,64473	-1,94784

3.6. Cole-Cole-Plot for the complex modulus E_1

In result of the interpretation of the triaxial tests, the Cole-Cole-Plot for a quasi uniaxial stress state for the complex modulus E_1 is illustrated in Fig. 12.

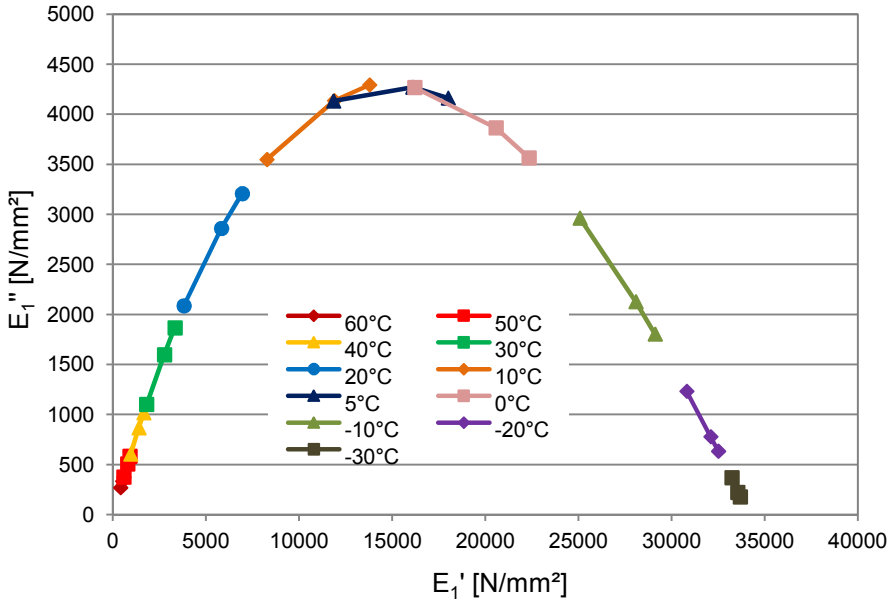

Fig. 12: Cole-Cole-Plot for the complex modulus E_1 with $\sigma_{23} = 0$ N/mm²

The complex modulus is composed by storage modulus E' and loss modulus E''

$$E = E' + i \cdot E'', \tag{22}$$

where $i = \sqrt{-1}$.

With the introduction of the stress component σ_{23}, the stress dependency of the complex modulus E_1 begins to appear (see Fig. 13). On higher temperatures and lower frequencies respectively lower temperatures and higher frequencies, the curves of the Cole-Cole-Plot lie upon each other. The boundary values consisting of the glassy modulus and the static modulus remain unaltered.

Between the boundary values, the curve of the complex modulus in dependency on σ_{23} tends to be more flat with increasing σ_{23}. This behaviour is caused by the interaction between the binder and the granular structure during the load transfer (see Section 3.3).

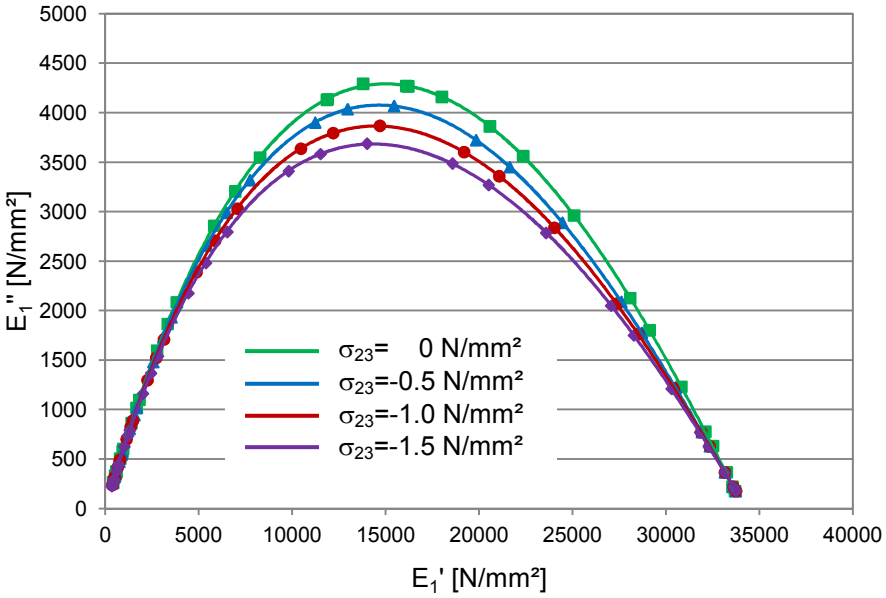

Fig. 13: Cole-Cole-Plot for the complex modulus E_1 with dependency on σ_{23}

3.7. Poissons's Ratio

In result of the interpretation of the uniaxial and triaxial tests, Poisson's ratio μ_1 versus the absolute modulus $|E_1|$ are shown in Fig. 14. For the regression of Poisson's ratio, the following functional approach [6]

$$\mu_1 = a_{1,\mu_1} + \frac{a_{2,\mu_1}}{1 + e^{(a_{3,\mu_1} + a_{4,\mu_1} \cdot \log_{10}(|E_1|))}} \tag{23}$$

is used.

The calculation of Poisson's ratio resulting from the triaxial test is limited due to problems with the radial measurement system. Hence, the results of the triaxial tests can only reflect the trend of Poisson's ratio and not determine the correct value. In this context, it is also currently impossible to verify a stress dependency of Poisson's ratio.

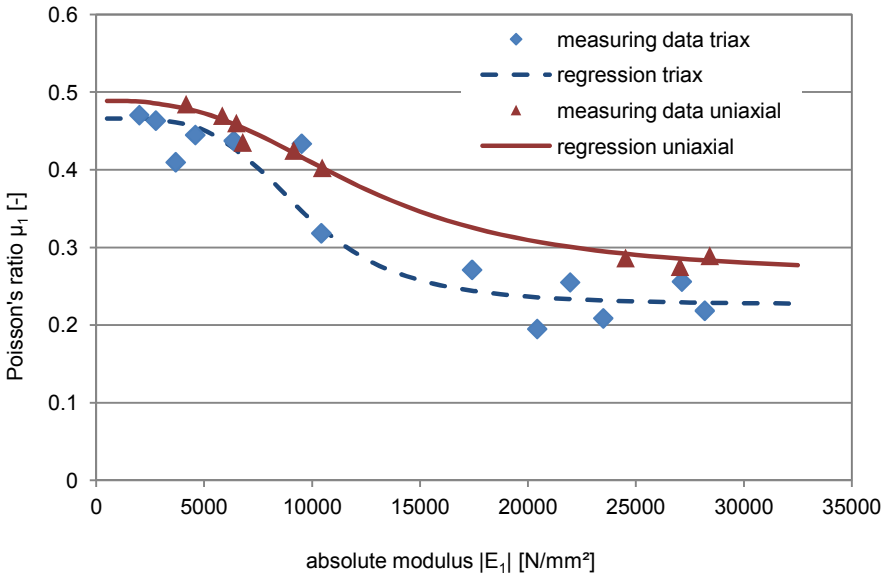

Fig. 14: Absolute modulus $|E_1|$ versus Poisson's ratio μ_1

In summary, Poisson's ratio can currently only be calculated by using the interpretation of the uniaxial test. The parameters of the regression function (23) are listed in Tab. 4.

Tab. 4: Parameters of regression function (23) for the uniaxial test

$a_{1,\mu1}$	$a_{2,\mu1}$	$a_{3,\mu1}$	$a_{4,\mu1}$
0.2635	0.2251	-26.7253	6.5298

4. NUMERICAL SIMULATION OF THE MATERIAL BEHAVIOUR OF ASPHALT

4.1. Fractional Material Model of Asphalt

The mechanical behaviour of asphalt depends on the mixture out of mineral aggregate and bituminous binder. All mineral aggregates are broken and sieved pieces of stones. They are rough solids with a large surface area. Hence, this large surface area leads to a high bonding between binder and aggregates. The bituminous binder is a highly viscous, ductile and temperature dependent fluid-like material. In case of compression, the stiffness of the asphalt compound is mostly influenced by the mineral aggregates and their interaction, like e.g. friction properties. Tensile stiffness of the compound is only influenced by the binder behaviour. During loading processes, the mineral aggregates are moving within the asphalt compound and the binder is under finite strains. The fluid-like behaviour of the binder leads to the viscous properties of the asphalt compound. Furthermore, irreversible, time-dependent distortions are obtained by the movement of the mineral aggregates.

The material description and characterisation of asphalt compounds as well as the determination of the material parameters are carried out based on the material test results. The development and realisation of all necessary material tests is described before. In order to model the material behaviour of asphalt in an adequate way, a material model based on finite strain theory is developed at ISD. The phenomenological rheology is shown in Fig. 15. The proposed material model consists of a dashpot and a fractional

Zener model in series [7], [8], [9], [10]. The dashpot controls the irreversible deformation. These irreversible deformations are rate-dependent. The fractional Zener model represents the viscoelastic material behaviour.

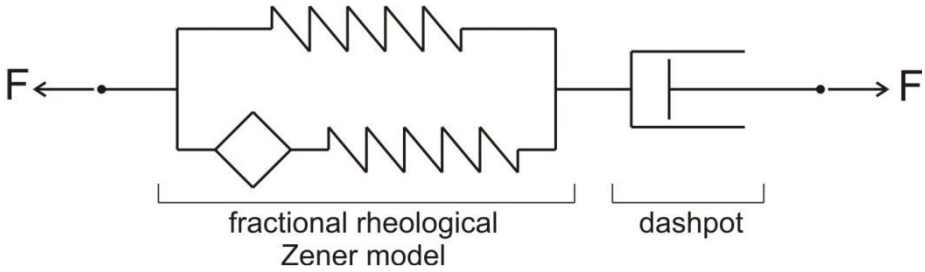

Fig. 15: Fractional rheological Zener model in series with a dashpot

Three cyclic tests of three different frequencies (1 Hz, 5 Hz and 10 Hz), with one stress amplitude ($\approx$ 1 N/mm²) and at one temperature (25°C) are used to fit a material parameter set for the asphalt mixture (SMA 11 S with PmB 25/55-55A). The determined set of material parameters for a temperature of 25°C is shown in Tab. 5. The large amount of material test data will be used for a further fitting of the material parameters especially under consideration of different temperatures.

Tab. 5: Detected material parameter set

C_{10}^{z} [N/mm²]	130.000	p [s]	2000.00
C_{10}^{e} [N/mm²]	1400.000	α [-]	0.95
D_1 [mm²/N]	0.001	η [s]	60000.00

4.2. Numerical Simulation of an asphalt test

The performance of the material model will be shown with a finite element (FE) simulation of an asphalt material test [11]. The specimen has cylindrical shape with a height of 300 mm and a diameter of 150 mm. During the test, the top of the specimen is subjected to a cyclic loading in longitudinal direction. The frequency of the loading is 1 Hz and the stress amplitude is 1 N/mm² (see Fig. 16).

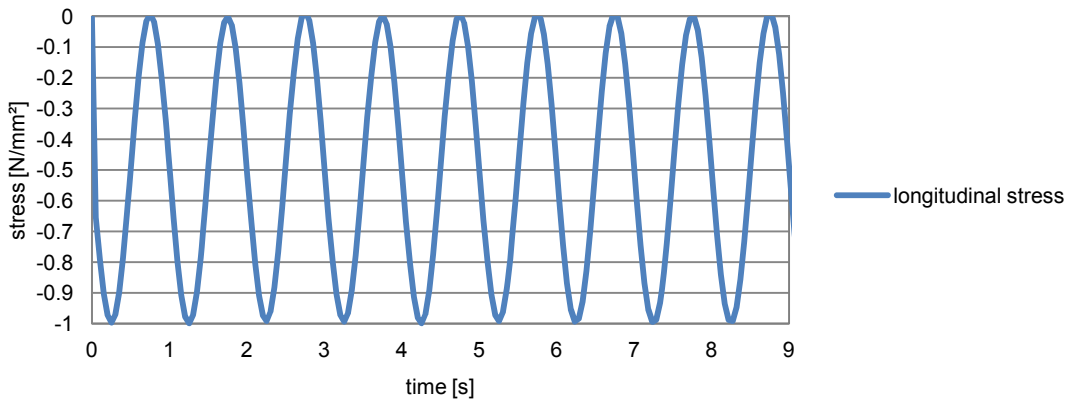

Fig. 16: Loading of the specimen

At the bottom of the specimen, all nodes are fixed. The nodes at the top of the specimen are only fixed in radial direction. The lateral surface of the cylindrical specimen is either fixed or loaded. For the simulation, the material parameters depicted in Tab. 5 are used. The geometry of the specimen is discretized by 728 three-dimensional standard 8-node isoparametric displacement elements with eight integration points per element. In Fig. 17, the increase of the longitudinal strain during the loading period is visible. In this figure, the specimen is completely unloaded at the five time steps. Therefore, the radial and longitudinal strains of the simulation and of the measured test data are compared in Fig. 18. The differences between the test and simulation results are marginal for the first five load cycles. Afterwards, the behaviour of the material model is slightly too soft.

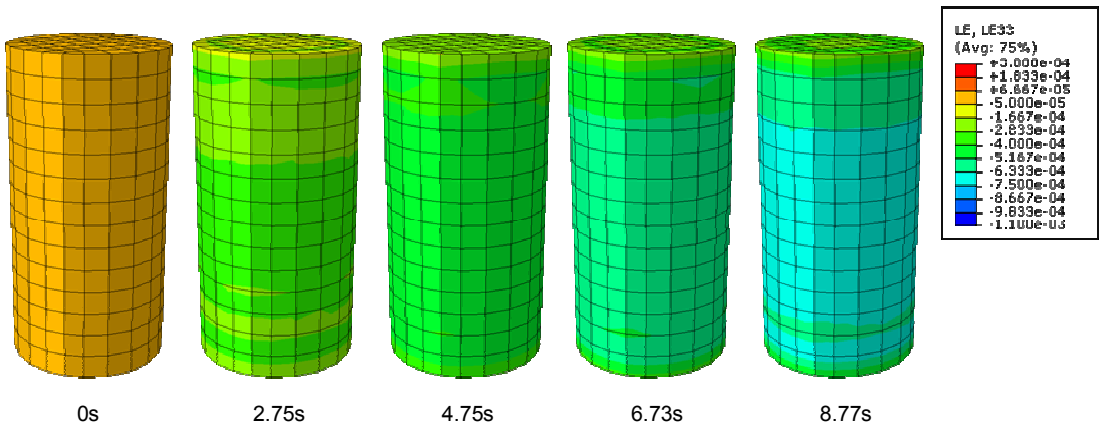

Fig. 17: Longitudinal strain at different time steps

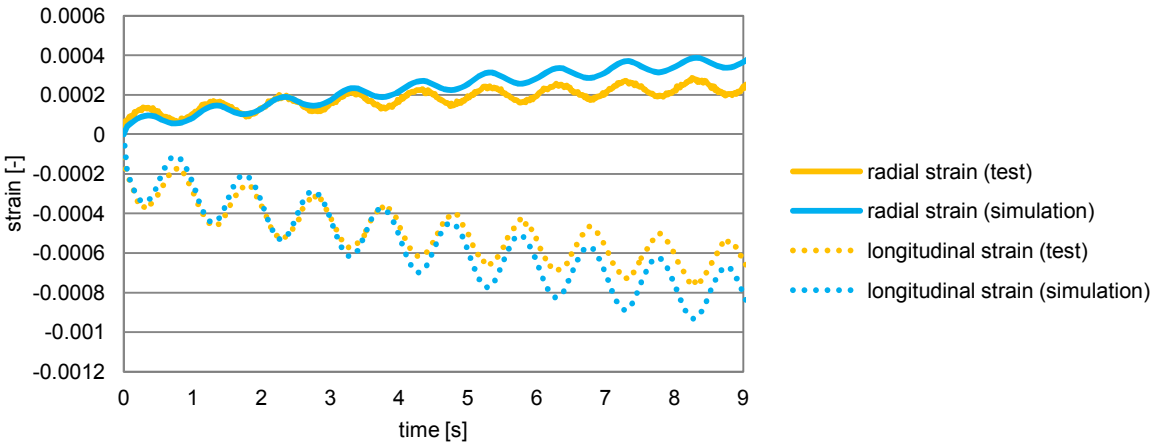

Fig. 18: Comparison between test and simulation of longitudinal and radial strains

5. SUMMARY

That the material behavior of asphalt depends on temperature and frequency is well-known. Furthermore, in result of the interpretation of the triaxial tests a stress dependent material behavior of asphalt may be detected. The influence of the stress state depends largely upon the temperature and affects higher frequencies more than lower frequencies.

For the numerical simulation of the load bearing behavior of asphalt and the determination of representative model parameters it is essential to describe the material behavior as realistically as possible. With the above listed approach it becomes possible to interpret the complex triaxial test and to detect the stress dependent material behavior of asphalt.

REFERENCES

1. Read, J., (1996). Fatigue Cracking of Bituminous Paving Mixtures. PhD-Thesis, University of Nottingham
2. Werkmeister, S.; Wellner, F. (2004). Investigation of the Fatigue Behavior of Asphalt Mixtures with the Dynamic Indirect Tensile Test in the Context of an Analytical Pavement Design (in German). Bitumen Heft 2
3. Werkmeister, S.; Wellner, F.; Oeser, M. (2006). Study on the Fatigue Behaviour of Asphalt Mixes Using the Dynamic Indirect Tensile Test within the Scope of Analytical Design. ISAP Conference
4. Weise, C.; Wellner, F.; Werkmeister, S. (2006). Determination of the Fatigue Behaviour of Asphalt Mixes using the Results of Direct, Indirect and Triaxial Tensile Tests. International Conference on Advanced Characterization of Pavement and Soil Engineering Materials, Athens, June 2007 (accepted)
5. Hürtgen, H. (2000). Methoden zur Beschreibung der thermomechanischen Eigenschaften von Asphalt (Asphalt-Rheologie). Fachgebiet Konstruktiver Straßenbau, Heft 20, Hannover
6. Maher, A.; Bennert, T. (2008). Evaluation of Poisson's Ratio for Use in the Mechanistic Empirical Pavement Design Guide (MEPDG). Final Report, New Jersey Department of Transportation
7. Zopf, C.; Kaliske, M. (2010). Constitutive description of green rubber material for forming simulation. In: Conference Proceeding of International Rubber Conference & Exhibition (IRC), pp. 170-173
8. Oeser, M.; Freitag, S.; Möller, B.; Wellner, F.; Werkmeister, S. (2006). 3-D Constitutive Model for Asphalt on the Basis of Fractional Creep Functions. In: Proceedings on the 10th International Conference on Asphalt Pavements (ISAP), CD-ROM, pp. 755-765
9. Schmidt, A.; Gaul, L. (2002). Finite Element Formulation of Viscoelastic Constitutive Equations Using Fractional Time Derivatives. Nonlinear Dynamics 29, pp. 37-55
10. Lion, A.; Kardelky, C. (2004). The Payne Effect in Finite Viscoelasticity: Constitutive Modelling Based on Fractional Derivatives and Intrinsic Time Scales. International Journal of Plasticity 20, pp. 1313-1345
11. Bathe, K.J. (1996). Finite Element Procedures. Prentice Hall, London